Signature of Nanodiamond in Raman Spectra: A Density Functional Theoretical Study

Dongju Zhang[†] and R. Q. Zhang*

Department of Physics and Materials Science, City University of Hong Kong, Hong Kong SAR, China

Received: August 14, 2004; In Final Form: March 2, 2005

Nanocrystalline diamond (NCD) has attracted great attention both experimentally and theoretically in the past few years. The identification of the presence and the amount of NCD in amorphous carbon film has been a challenging issue. Although Raman spectroscopy has become a standard tool for the characterization of various carbon phases, a simple criterion for identifying NCD has not yet been well-established. In the present work, a theoretical study of the Raman spectra of the model compounds of NCD is presented on the basis of the density functional calculations. The reliability of the computational approach has been tested by comparing the predicated Raman spectra of several reference molecules to those obtained experimentally. To show the unique Raman spectrum of a NCD phase, a series of the model compounds of various carbon materials including tetrahedral and hexagonal clusters, and *trans*-polyacetylene fragments, were considered, and subsequently their Raman spectra below 2000 cm^{-1} were calculated and compared with each other. The calculated results indicate that the relatively stronger broad peak at about 480 cm^{-1} could be used as the signature of a NCD phase in the sample.

1. Introduction

Carbon is a most unique element that can give rise to materials as diverse as diamond, graphite, fullerenes, carbon nanotubes, and nanostructured disordered and amorphous carbons. These materials have various possible applications due to their remarkable mechanical, electronic, and chemical properties.[1−3] In the past few years, nanocrystalline diamond (NCD) has attracted great attention from both experimental and theoretical studies[4−6] because of its potential application as X-ray lithography masks, ultrathin and ultrahard antifriction coatings, nanocomposites, nanobearings, optical coatings, and insulating or semiconducting layers in electronic devices.[7−10] Recently, NCD films of 5−100 nm in size have been realized by chemical vapor deposition.[11−13] The properties of NCD are expected to be very different from those of the bulk due to its large surface-to-volume ratio. It is thus very useful to establish fast, reliable, and nondestructive techniques to probe the unique properties of this material. In addition to X-ray and transmission electron microscopy, Raman spectroscopy has become a popular tool for the structural characterization of carbon phases.[14−17] It is traditionally carried out at wavelengths in the blue-green spectral region; however, multiwavelength Raman studies have recently attracted a great deal of interest in characterizing the phonon modes of the different allotropes and noncrystalline phases of carbon. For example, it has been used to understand the nature of various carbon phases, including disordered, amorphous, and diamond-like carbons.[18] Given the unique property of NCD, it would be of interest to find its characteristic phonon modes that are different from those of hexagonal carbon clusters and *trans*-polyacetylene fragments which may be present in the deposited film. It is known that the Raman spectra of diamond films show a strong sharp peak at 1332 cm^{-1}, if any, with broad *D*- and *G*-mode peaks of amorphous carbon at 1350 and 1580 cm^{-1}, respectively. The Raman spectra of NCD films additionally show a mode at 1140 cm^{-1} and a peak at 1480 cm^{-1} appearing as a shoulder of the *G* mode. These two peaks, in particular the lower of them, are usually considered as characteristic signatures of NCD as they are not visible in the spectra of microcrystalline diamond films.[5,19,20] However, Pfeiffer et al.[6] attributed the Raman peak at 1140 cm^{-1} to the contribution of *trans*-polyacetylene in NCD films by measuring the Raman spectra of deuterated NCD films produced from a $D_2/CD_4/Ar$ plasma. Recently, Prawer and co-workers[5] reported the Raman signature of nanodiamond clusters of about 5 nm in diameter, where a strong broad peak at about 500 cm^{-1} was shown besides the common first-order diamond Raman line. By comparing the observed spectrum of nanodiamond clusters with that of amorphized diamond and with the calculated vibrational density of states of diamond, they proposed that the broad peak at 400−500 cm^{-1} originating from the breakdown of the selection rules is the fingerprint of a NCD phase in the sample.

In contrast to the extensive experimental research, there are few theoretical Raman data for a NCD phase. This paper aims to fill this deficiency by calculating Raman spectra of tetrahedral carbon clusters that model a NCD phase using density functional theory (DFT). The results are expected to help establish a criterion for distinguishing NCD from the hexagonal clusters and *trans*-polyacetylene fragments.

2. Modeling and Computational Approach

In this study, a series of tetrahedral (sp^3-bonded) carbon cluster models, $C_{10}H_{16}$, $C_{12}H_{18}$, $C_{14}H_{20}$, $C_{18}H_{24}$, $C_{26}H_{30}$, $C_{35}H_{36}$, and $C_{44}H_{42}$, as shown in Figure 1, were selected for calculations. These cluster models were extracted from the 3D structure of diamond to model a NCD phase. For comparison, hexagonal carbon clusters and *trans*-polyacetylene fragments were also selected for calculations. Figure 2 shows the models of the hexagonal clusters, C_6H_6, $C_{10}H_8$, $C_{14}H_{10}$, $C_{16}H_{10}$, $C_{24}H_{12}$, $C_{32}H_{14}$, and $C_{42}H_{16}$. The *trans*-polyacetylene fragments used here can

* To whom correspondence should be addressed. E-mail: aprqz@cityu.edu.hk.

† On leave from the School of Chemistry and Chemical Engineering, Shandong University, Jinan, Shandong 250100, China.

10.1021/jp046330d CCC: $30.25
Published on Web 04/07/2005

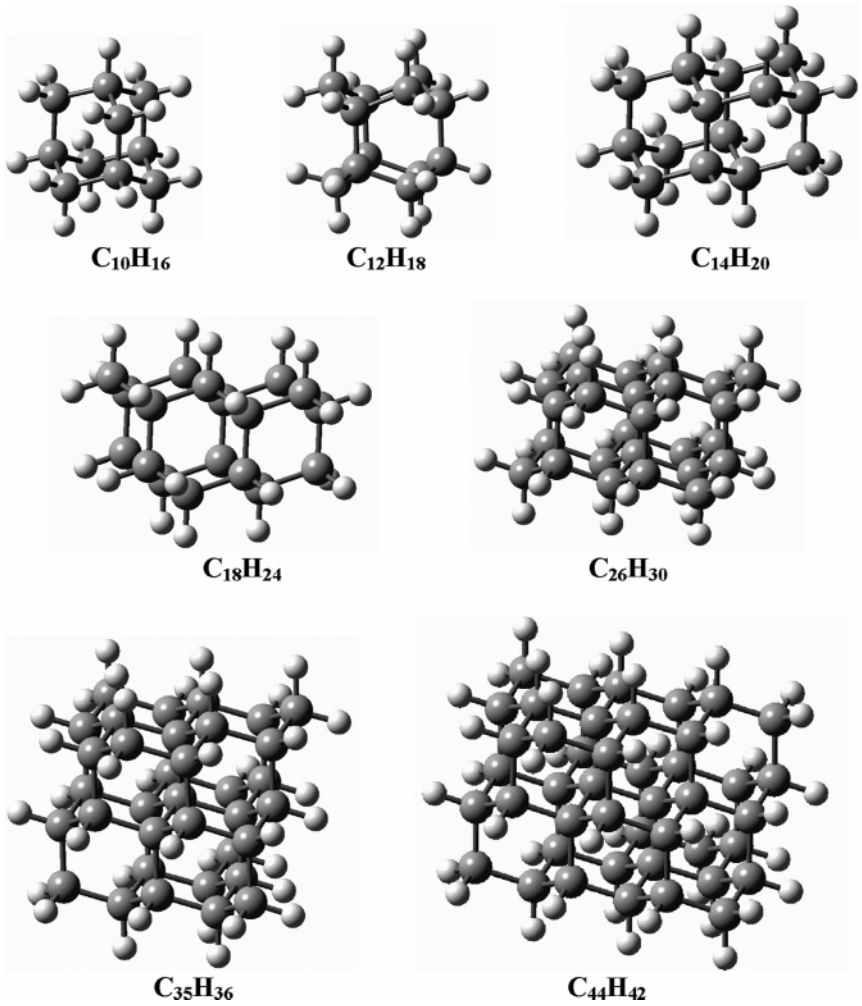

Figure 1. Tetrahedral carbon clusters based on the diamond lattice to simulate nanocrystalline diamond. The boundary carbon atoms were saturated with hydrogen atoms for each cluster.

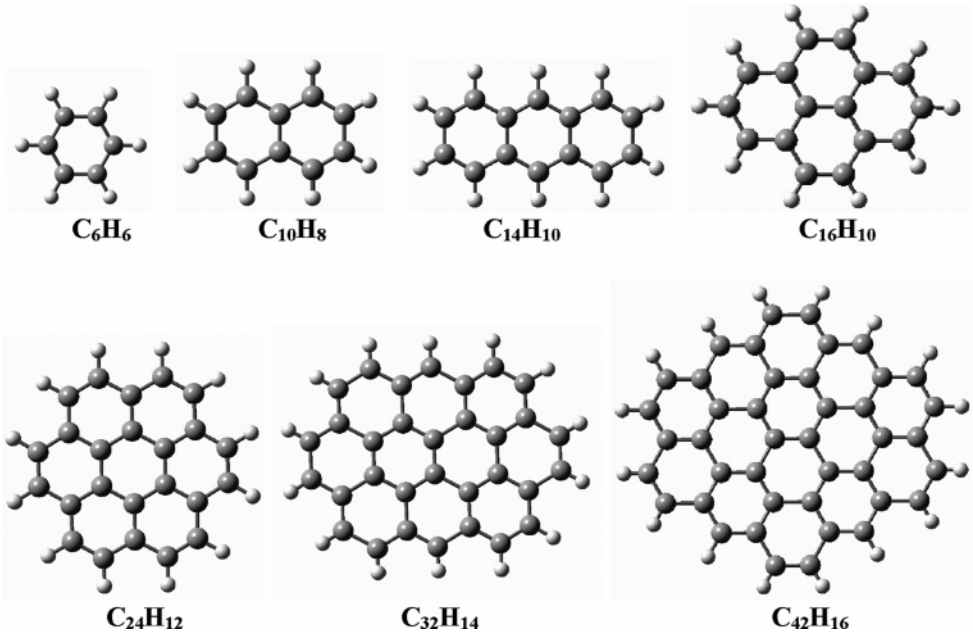

Figure 2. Hexagonal carbon clusters. The boundary carbon atoms were saturated with hydrogen atoms.

be expressed as C_nH_{n+2} (n = 6, 8, 10, 12, 14, 16, and 18). Their structures are simple and are thus not shown here. For all these tetrahedral and hexagonal carbon clusters, and *trans*-polyacetylene fragments, hydrogen atoms were used to saturate the dangling bonds at the boundaries based on their known crucial effect in stabilizing sp^3-bonded carbon networks. Despite their small sizes, these models are expected to show the trend in C−C bond vibrational signals (frequencies and intensities) with

TABLE 1: Calculated Raman Frequencies (cm^{-1}) and Raman Scattering Activities (in Parentheses ($Å^4$ amu^{-1})) for C_2H_6 and C_2H_4 Molecules Using the B3LYP Functional with Different Basis Sets

		6-31G(d)	6-31+G(d)	6-311+G(d)	cc-pvtz	aug-cc-pvtz	exptl[a]
C_2H_6	$1a_g$	3047	3041	3027	3026	3025	2914
		(208.99)	(255.26)	(269.62)	(292.44)	(355.55)	(360.1 ± 77.3)
	$2a_g$	1454	1446	1436	1423	1421	1406
		(7.94)	(2.27)	(2.14)	(1.02)	(0.02)	(2.2 ± 2.0)
	$3a_g$	1010	1004	1001	995	994	1000
		(8.69)	(13.80)	(12.56)	(11.06)	(12.29)	(16.9 ± 1.7)
	$1e_g$	3098	3088	3088	3070	3068	2967
		(270.28)	(295.00)	(291.82)	(138.61)	(255.58)	(170.42 ± 42.8)
	$2e_g$	1532	1525	1521	1504	1502	1475
		(79.98)	(43.02)	(42.16)	(36.04)	(17.10)	(18.3 ± 4.6)
	$3e_g$	1235	1229	1226	1223	1222	1202
		(6.34)	(2.26)	(1.26)	(0.61)	(0.17)	(≤0.46)
C_2H_4	$1a_g$	3167	3162	3137	3140	3139	3026
		(184.87)	(198.21)	(200.18)	(219.05)	(217.44)	(172.5 ± 26.9)
	$2a_g$	1721	1701	1693	1693	1689	1630
		(6.69)	(33.07)	(31.52)	(13.32)	(33.15)	(17.6)
	$3a_g$	1396	1389	1383	1382	1381	1342
		(35.29)	(40.39)	(39.85)	(34.85)	(42.82)	(26.0 ± 3.3)
	$1b_{3g}$	3222	3218	3194	3195	3194	3102
		(121.83)	(127.86)	(124.19)	(128.71)	(123.90)	(66.9 ± 14.2)
	$2b_{3g}$	1248	1244	1248	1247	1246	1220
		(1.67)	(1.27)	(0.80)	(0.35)	(0.07)	(≤2.9)
	B_{2g}	956	964	961	984	985	940
		(0.63)	(3.82)	(2.28)	(2.05)	(3.32)	(1.6)

[a] The experimental values are from ref 26 for C_2H_6 and from ref 27 for C_2H_4.

increasing cluster size in different carbon materials. The dangling bonds at the cluster model boundaries were all saturated using hydrogen atoms to simulate the environment of the carbon domains in a film where an amorphous carbon matrix provides a similar saturation. This is the reason the H to C ratios in these models, in particular in the tetrahedral clusters, are higher than that in a nanodiamond film. As in the region around 500 cm^{-1}, the region where the signature of a NCD phase is to be established in the present work, the vibrational modes of the CH, CH_2, and CH_3 groups are absent, the presence of these C−H bonds at the cluster boundary does not detract from our intention.

Our calculations were carried out using the Becke three-parameter and Lee−Yang−Parr functionals (B3LYP) of density functional theory.[21−23] It has been demonstrated that the vibrational spectra of carbon materials determined at this theoretical level agree well with experimental data.[24] Recently, Neugebauer[25] et al. evaluated the validity of DFT for the calculation of Raman spectra for large molecules by comparing the Raman activities obtained from DFT calculations with those from highly correlated ab initio methods and experimental data. They again concluded that the B3LYP is a reliable method for predicting Raman intensities which gives sufficient accuracy even when medium-sized basis sets are used.

To accurately predict the Raman spectra of carbon materials with a reasonable computational cost, it is crucial to select an appropriate basis set combination with the B3LYP functional. We preformed calculations at first for two reference compounds, C_2H_6, and C_2H_4, using the B3LYP approach with different basis sets, including medium-sized basis sets, such as the 6-31G(d), a split-valence atomic basis set supplemented by a polarization function and large-sized basis sets, such as the Dunning's correlation consistent basis sets, cc-pVTZ and aug-cc-pVTZ. Those two small molecules possess C−C and C═C bonds, respectively, allowing the inspection of the reliability of the B3LYP/6-31G(d) method in predicting the corresponding vibrational modes. Table 1 lists the calculated Raman frequencies and Raman scattering activities (in parentheses) by combining the B3LYP approach with different basis sets, including 6-31G(d), 6-31+G(d), 6-311+G(d), cc-pVTZ, and aug-cc-pVTZ. The corresponding experimental results were also given in Table 1 for comparison.

It can be seen from Table 1 that the theoretical calculations reproduce fairly well the experimental Raman frequencies of these molecules. As expected, all of the calculated wavenumbers are shifted upward (most within 30 cm^{-1}) with respect to the experimental ones. This can be attributed to the harmonic oscillator approximations and the insufficient inclusion of electron correlation effects in the adopted approaches. There is a discrepancy in the calculated relative Raman intensities compared to the experimental values, which is commonly attributed to experimental uncertainties[28] and the limitations of Placzek's polarizability theory.[29] Nevertheless, this does not affect the present intention, since our main aim here is to find the characteristic position of a NCD phase, not to calculate the accurate Raman intensities. The increase of the basis set does not significantly improve the relative Raman intensities. Dunning's aug-cc-pVTZ basis set gives better results than others. However, this basis set is not routinely feasible in Raman spectrum calculations for larger molecules because of computational expensiveness. On the other hand, we found that even the medium-sized basis set, 6-31G(d), reproduced fairly well the order of relative Raman intensities. And this order is also in good agreement with that obtained with the aug-cc-pVTZ basis set. Further, we compared the Raman spectra of several small carbon clusters, sp^3-bonded C_5H_{12} and sp^2-bonded C_3H_5, C_4H_6, and C_5H_7, at the B3LYP/6-31G(d) level with those at the B3LYP/aug-cc-pVTZ level. Figure 3 shows the computed spectra below the wavenumber 2000 cm^{-1}. It can be seen that the two basis sets predict almost the same Raman frequencies, although there are discrepancies in the relative intensities, in particular for sp^3-bonded C_5H_{12}. However, the 6-31G(d) basis set is expected to produce relative Raman intensities similar to those of the aug-cc-pVTZ basis set as the size of the sp^3-bonded cluster increases, as shown in Figure 3 for the sp^2-bonded clusters. Moreover, Table 2 compares the computed results (only frequencies in view of the lack of the accurate Raman intensities) using the 6-31G(d) basis set for C_4H_6, a representative of these

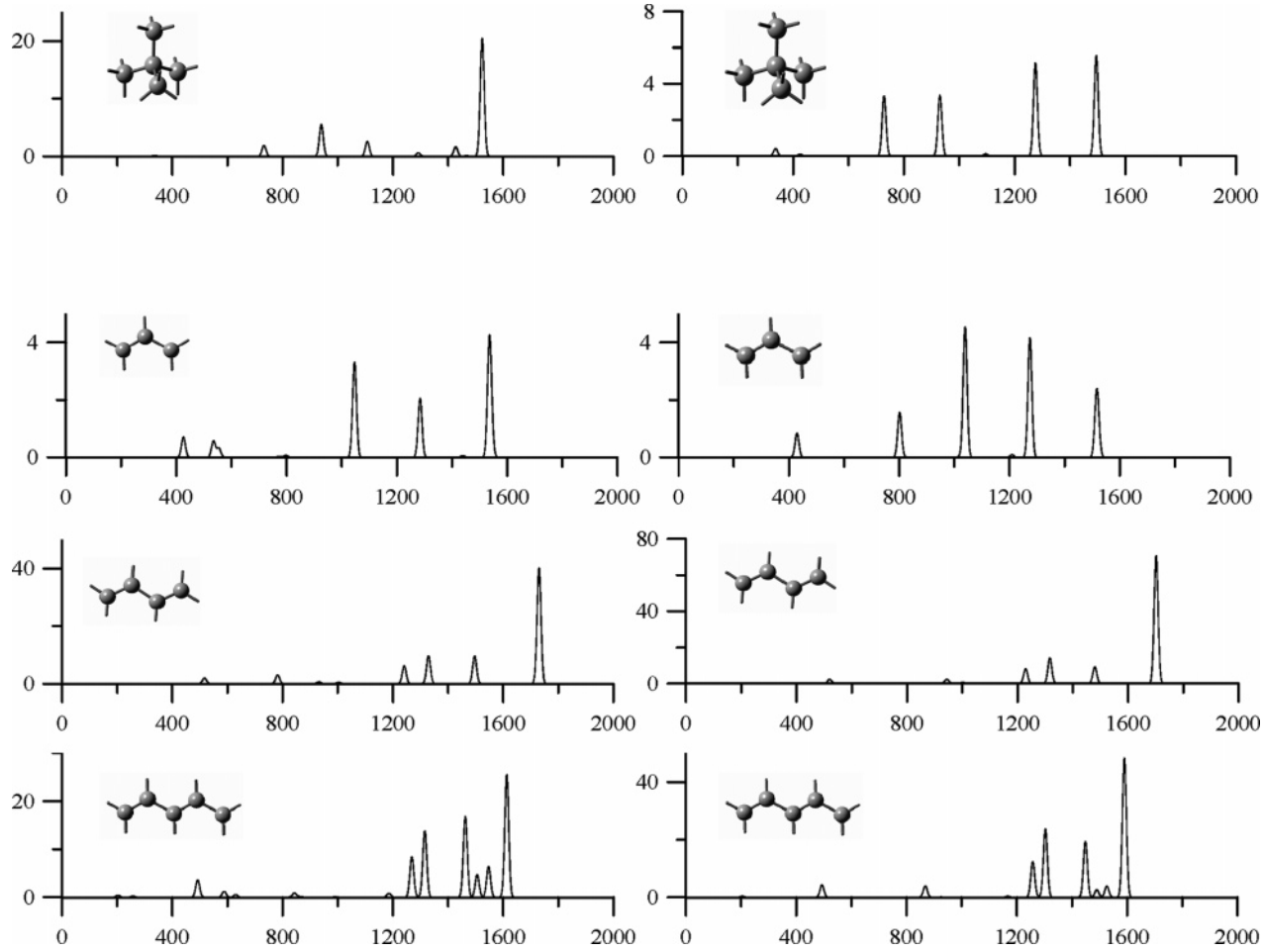

Figure 3. Comparison of the Raman spectra of several representative molecules within wavenumbers below 2000 cm^{-1}, calculated form the B3LYP approach with 6-31G(d) (on the left) and aug-cc-pvtz (on the right). Harmonic frequencies (horizontal axes) and Raman scattering activities or intensive (vertical axes) are in cm^{-1} and $Å^4$ amu^{-1}, respectively.

TABLE 2: Calculated and Experimental Frequencies of Butadiene (cm^{-1}) at the B3LYP/6-31G(d) Level

calcd[a]	exptl[b]	calcd[a]	exptl[b]
172	163[c]	1296	1279
294	301	1308	1294
509	513	1401	1381
526	535	1459	1441
761	754	1610	1579
880	887	1660	1644
930	905	3025	2986
930	908	3036	3014
985	974	3045	3025
996	988	3045	3062
1032	1022	3130	3103
1212	1206	3131	3105

[a] Scaled by the factor 0.9614. [b] Taken from ref 30. [c] Taken from ref 31.

clusters, to the corresponding experimental values, and fairly good agreement is observed again. These preliminary calculations give us the confidence to use B3LYP with the medium-sized 6-31G(d) basis set in calculations of Raman spectra for carbon clusters. The reliability of this level of theory in predicting Raman activities and frequencies was also shown in a recent work in which experimental results of C_{60} were compared.[32] Thus the following calculations will be performed at the B3LYP/6-31G(d) level of theory.

All of the model compounds studied in this work were fully optimized at the B3LYP/6-31G(d) level of theory. The optimized geometries were used to calculate the harmonic vibrational frequencies and the derivatives of components of the polarizability tensor, based on which the Raman intensities are evaluated within the double harmonic approximation.[33] This approximation assumes a harmonic force field and ignores quadratic and higher terms in the series expansion of the polarizability tensor components with respect to a vibrational normal mode. All of the calculations were performed using Gaussian 98 code.[34]

3. Results and Discussion

According to previous computational experiences, vibrational frequencies computed at the B3LYP/6-31G(d) level tend to be around 1−4% too high. Thus, the B3LYP/6-31G(d) frequencies should be scaled by multiplying a correction factor of 0.9614 to obtain better estimates of the experimental results.[35] Figure 4 displays the scaled Raman spectra of the tetrahedral carbon clusters with the wavenumber below 2000 cm^{-1}. The following spectral features are obvious: (i) the spectra become well-regulated with increasing cluster size, and the strongest peaks occur at the vicinity of 1200 and 1500 cm^{-1}; (ii) the peak at the region of 350−550 cm^{-1} clearly emerges as the cluster size reaching up to $C_{26}H_{30}$; (iii) there are no vibrational modes at energies exceeding about 1500 cm^{-1}; and (iv) the Raman intensities are very weak for the sp^3-bonded clusters and are not sensitive to the cluster size.

We now discuss these features. First of all, we focus our attention on the two strongest peaks at about 1200 and 1500 cm^{-1}. These two peaks seem to be relevant to the conventionally

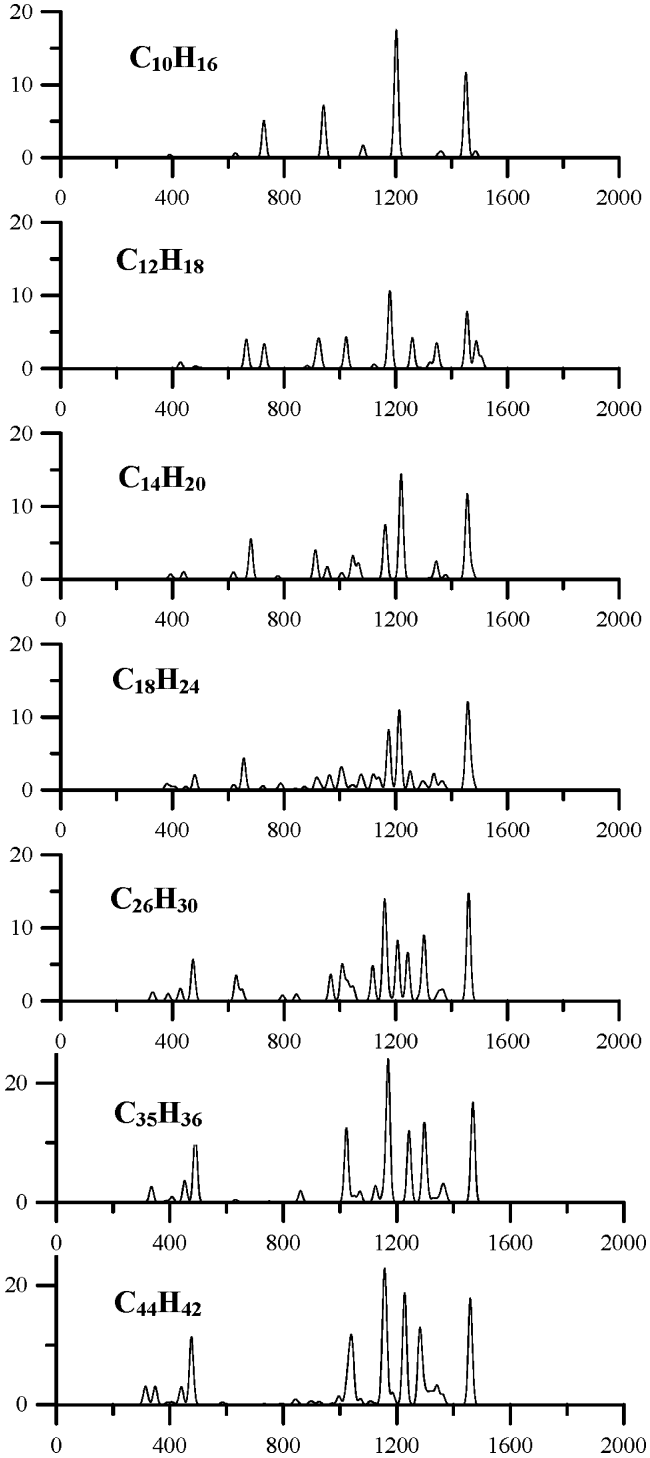

Figure 4. Scaled Raman spectra with wavenumbers below 2000 cm^{-1} for the tetrahedral carbon clusters shown in Figure 1, calculated at the B3LYP/6-31G(d) level of theory.

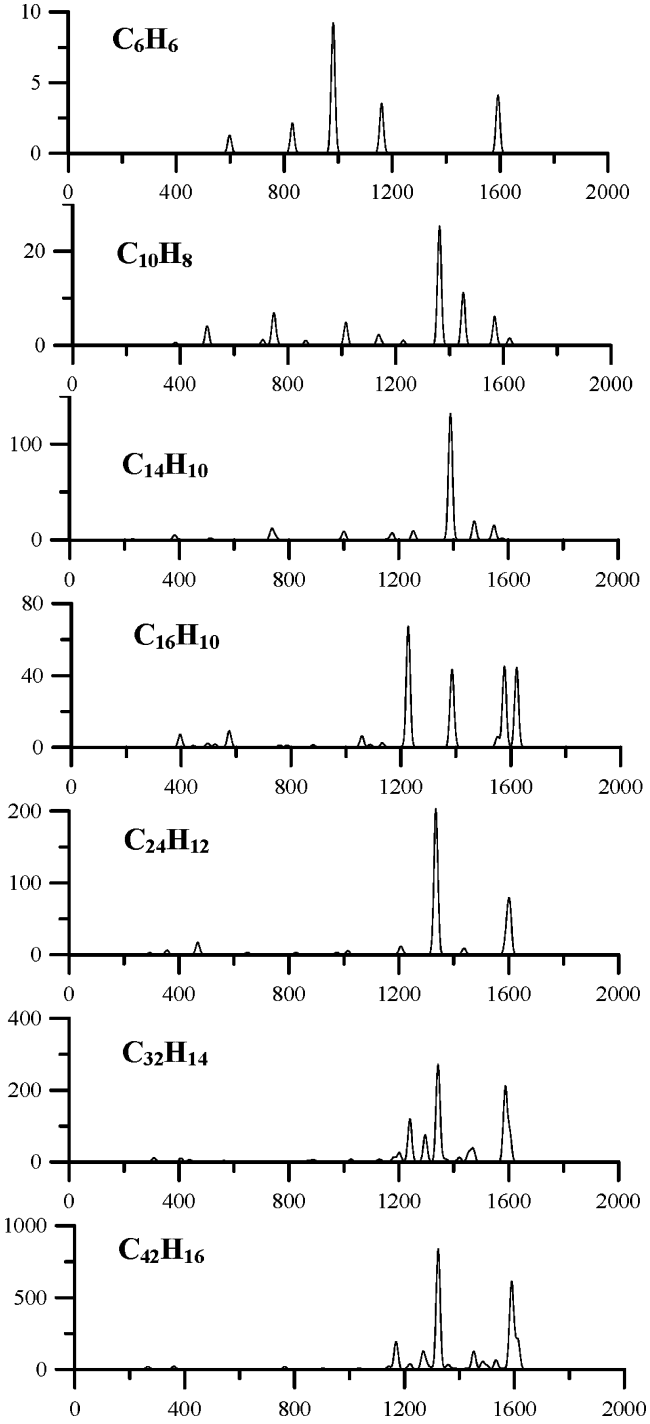

Figure 5. Scaled Raman spectra with wavenumbers below 2000 cm^{-1} for the hexagonal carbon clusters shown in Figure 2, calculated at the B3LYP/6-31G(d) level of theory.

assigned characteristic modes of NCD at 1140 and 1480 cm^{-1}. However, they also appear together for *trans*-polyacetylene fragments and even for sp^2-bonded clusters, as observed in early experiments.[36,37] Furthermore, the Raman intensities for the latter two at the vicinity of these wavenumbers are much stronger than those for sp^3-bonded structures and thus will swamp the signal from the latter. As a theoretical confirmation, Figures 5 and 6 show the scaled Raman spectra of the hexagonal carbon clusters and the *trans*-polyacetylene fragments, respectively. For the former, we note that there are strong Raman vibrational modes at energies from about 1200 to 1700 cm^{-1}. While for the latter, there are two very sharp peaks appearing at about 1200 and 1600 cm^{-1}, which obviously correlate with the experimentally observed C−H bending mode (1140 cm^{-1}) and the C═C stretch mode (1480 cm^{-1}), respectively. These facts indicate that the assignments of 1140 and 1480 cm^{-1} modes to a NCD phase are not without problems because of their weak intensities and nonpeculiar Raman scatterings. These two modes were recently confirmed experimentally by Kuzmany et al. to originate from *trans*-polyacetylene in the diamond film, by performing a thin film preparation with deuterium and H−D substituted hydrocarbon sources.[38]

The second feature of the sp^3-bonded carbon clusters is the peak at the region of 350−550 cm^{-1}. In the experiment carried

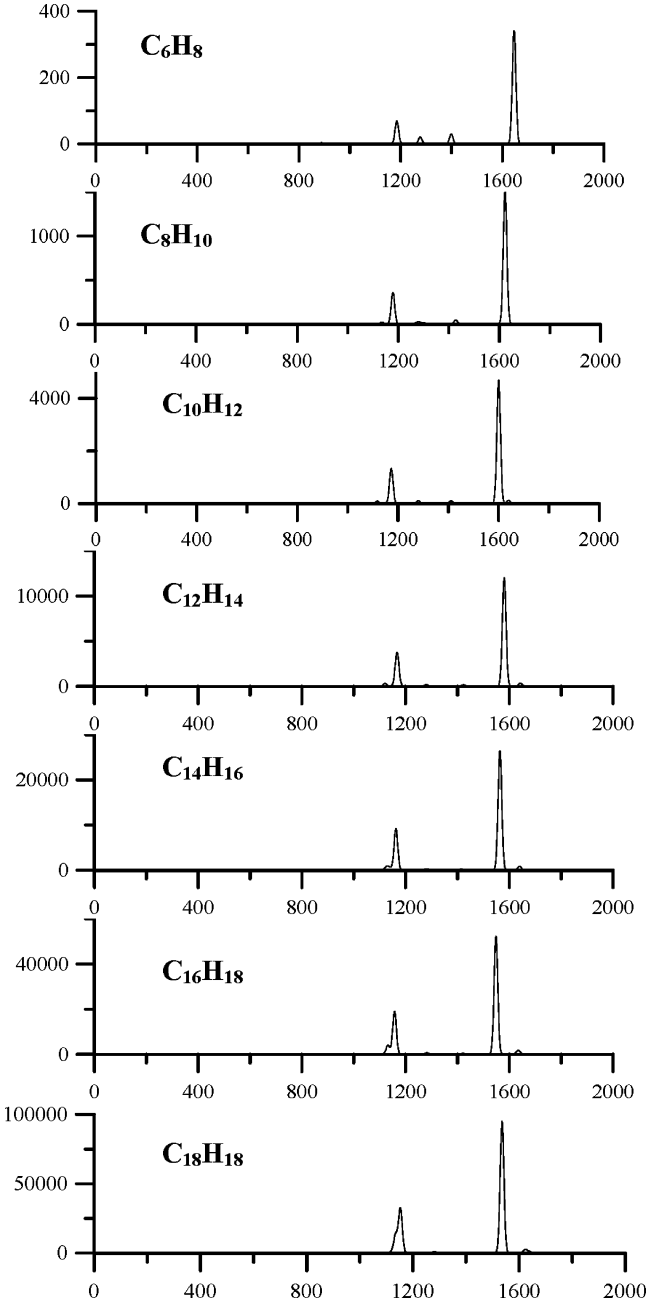

Figure 6. Scaled Raman spectra with wavenumbers below 2000 cm^{-1} for several *trans*-polyacetylene fragments (-(CH−CH)$_x$-) calculated at the B3LYP/6-31G(d) level of theory.

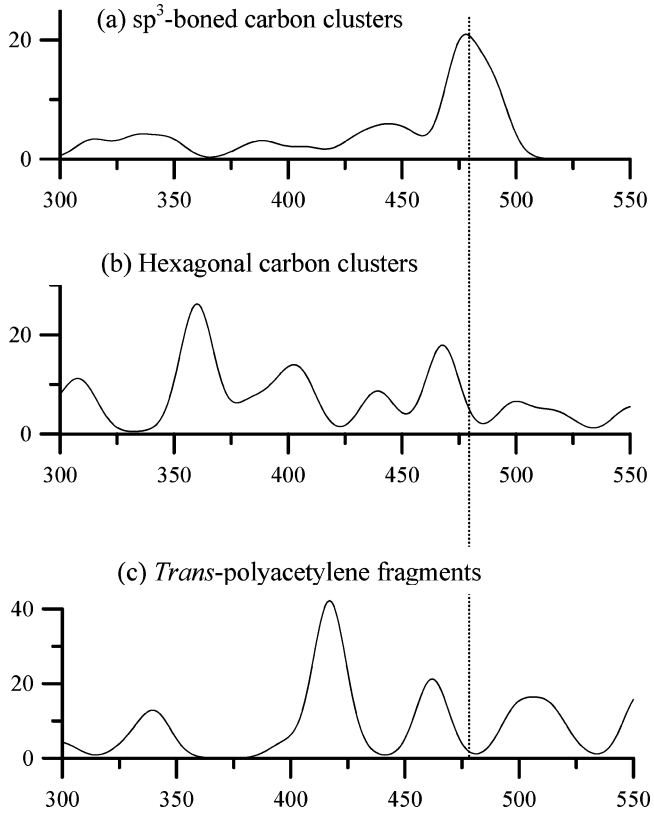

Figure 7. Sum of the Raman intensities for the various-sized (a) tetrahedral clusters, (b) hexagonal clusters, and (c) *trans*-polyacetylene fragments in the 350−550 cm^{-1} region, respectively.

out by Prawer et al.,[5] NCD showed a strong broad peak at 400−500 cm^{-1}. The present calculations reproduce well the experimental finding. However, the question as to whether this peak can be used as a criterion for a NCD phase has to be further investigated by comparing its Raman spectra to those of hexagonal carbon clusters and *trans*-polyacetylene fragments, which might possibly be formed during the deposition of diamond films. Our calculations show that the sp^2-bonded clusters, i.e. the hexagonal carbon clusters (Figure 5), and the *trans*-polyacetylene fragments (Figure 6) also have small Raman signals in the vicinity of this area, which seems to make the assignment of NCD modes somewhat doubtful at this region. However, we found that the accurate positions and fingerprints of the Raman signatures for the former two differ from those of the latter. To reveal the characteristic signals of the tetrahedral and hexagonal clusters as well as the *trans*-polyacetylene fragments at this region, we summed the intensities of various-sized tetrahedral and hexagonal clusters at the 300−550 cm^{-1} region, respectively, the calculated results for which are shown in Figure 7. At the vicinity of 480 cm^{-1}, the summed Raman spectrum for the tetrahedral clusters has a strong broad peak (Figure 7a), which is in good agreement, about both the shape and position of the peak, with the experimental Raman spectra of nanodiamond powder carried out by Prawer et al.[5] This feature is clearly different from those of the hexagonal carbon clusters and *trans*-polyacetylene fragments. As shown in Figure 7b, the hexagonal carbon clusters have a most sharp peak at about 365 cm^{-1}, a weaker peak at about 465 cm^{-1}, and hardly any peak at 480 cm^{-1}. Clearly, the former two peaks cannot swamp the signal from the tetrahedral clusters at this region. For the *trans*-polyacetylene fragments (Figure 7c), two features of the Raman spectrum at this region are obvious: this spectrum is dominated by the peak at about 420 cm^{-1}, and there are hardly any vibrational modes in the vicinity of 480 cm^{-1}. The former may be the fingerprint of *trans*-polyacetylene fragments in this region, while the latter indicates that *trans*-polyacetylene fragments do not disturb the signal from the sp^3-bonded carbon clusters at about 480 cm^{-1}. Thus, by comparing the fingerprint characters of three types of carbon clusters, we confirm that the broad peak at about 480 cm^{-1} can be used as a criterion for a NCD phase in the sample. The origin of this peak can be attributed to the breakdown of the selection rules resulting from the uncertainty in the phonon momentum as the crystallite size is reduced. We now discuss (i) the effect of the cluster sizes of the model NCD, (ii) the effect of the hydrogen at the boundary, and (iii) the possible contribution from fullerenes to the proposed feature of NCD at around 480 cm^{-1}. First, it is clear from Figure 4 that there is a trend in the evolution of the feature in the vicinity of 480 cm^{-1} with increasing cluster size. From this,

we surmise that this feature holds in synthesized NCDs. Second, it is generally accepted and was confirmed by the present calculations again that the vibrational modes for the CH, CH_2, and CH_3 groups are in the regions of 1450−1475, 1300−1350, and 2800−2980 cm^{-1}, respectively. Thus, their contribution at around 480 cm^{-1} is ruled out. Third, the fingerprints of fullerenes at around 480 cm^{-1} are different from that of the sp^3-bonded carbon clusters: the former present a very sharp peak,[39,40] while the latter presents a broad peak. Furthermore, it should be noted that the fullerenes and nanodiamond were synthesized under very different conditions: the former were conveniently realized using carbon arcs[41] and combustion methods,[42] while the latter is generally grown by various chemical vapor deposition techniques.[43−45] To the best of our knowledge, fullerenes have never been observed to occur as incidental byproducts during nanodiamond growth, and vice versa. Based on these clarifications, the broad Raman peak at around 480 cm^{-1} may be considered as a criterion for identifying a NCD phase.

We now return to the other two features of the Raman spectra of the tetrahedral carbon clusters found in the present calculations. One is that there are no vibrational modes at energies of more than 1500 cm^{-1}. This feature is consistent with the previous calculations of the vibrational density of states (VDOS) of diamond.[46,47] Due to the reduced crystallite size, the phonon modes of the nanocrystalline materials are localized. As the last feature, the Raman intensities of the tetrahedral carbon clusters are very weak at the entire region within 2000 cm^{-1}. Furthermore, as shown in Figure 4, the Raman intensities are not sensitive to the cluster size. In contrast, by comparing Figure 4 and Figures 5 and 6, we find that the Raman spectra of the hexagonal carbon clusters and *trans*-polyacetylene fragments, in particular the latter, are much stronger than those of tetrahedral carbon clusters. And their intensities show a large dependence on the cluster size: the Raman intensity increases remarkably with the increasing cluster size. These facts are also in good agreement with previous Raman studies of NCD materials. Thus, given the larger Raman cross-section for sp^2-bonded clusters due to resonance effects, it is clear that the interesting features of NCD spectra can be marked by the strong signals from the former, which explains the experimental difficulty of finding a criterion for identifying a NCD phase. However, as emphasized above, we have confirmed that the relatively stronger broad peak at about 480 cm^{-1} can be used as a characteristic signal of a NCD phase since it is not visible in the spectra of hexagonal carbon clusters and *trans*-polyacetylene fragments in this region. It should be emphasized that the Raman frequencies and intensities of the tetrahedral carbon clusters are not significantly sensitive to the cluster size.

4. Conclusions

We have studied the Raman spectra of a series of carbon clusters modeling a NCD phase by performing calculations at the B3LYP/6-31G(d) level of density functional theory. We found that the Raman spectra of the tetrahedral carbon clusters were not significantly sensitive to its size. A relatively stronger board peak at about 480 cm^{-1} has been established as a criterion for identifying a NCD phase by comparing the Raman spectra of the sp^3-bonded clusters to those of the sp^2-bonded clusters.

Acknowledgment. The work described in this paper was supported by grants from the City University of Hong Kong (Project No. 7001449) and CAS-Croucher Funding Scheme for Joint Laboratories.

References and Notes

(1) Robertson, J. *Pure Appl. Chem.* **1994**, *66*, 1789.
(2) Robertson, J. *Adv. Phys.* **1986**, *35*, 317.
(3) Dresselhaus, M. S.; Dresselhaus, G.; Eklund, P. C. *Science of Fullerenes and Carbon Nanotubes*; Academic Press: New York, 1996.
(4) Greiner, N. R.; Philips, D. S.; Johnson, J. D.; Volk, F. *Nature* **1988**, *333*, 440.
(5) Prawer, S.; Nugent, K. W.; Jamieson, D. N.; Orwa, J. O.; Bursill, L. A.; Peng, J. L. *Chem. Phys. Lett.* **2000**, *332*, 93.
(6) Pfeiffer, P.; Kuzmany, H.; Salk, N.; Gunther, B. *Appl. Phys. Lett.* **2003**, *82*, 4149.
(7) Yarbrough, W. A.; Messier, R. *Science (Washington, D.C.)* **1990**, *247*, 688.
(8) Windischmann, H.; Epps, G. F. *J. Appl. Phys.* **1990**, *68*, 5665.
(9) Bachmann, P. K.; Lade, H.; Leers, D.; Wiechert D. U.; Theunissen, G. S. A. M. *Diamond Relat. Mater.* **1994**, *3*, 799.
(10) Erz, R.; Dotter, W.; Jung, K.; Ehrardt, H. *Diamond Relat. Mater.* **1993**, *2*, 449.
(11) Konov, V. I.; Smolin, A. A.; Ralchenko, V. G.; Pimenov, S. M.; Obraztsova, E. D.; Loubnin, E. N.; Metev, S. M.; Sepold, G. *Diamond Relat. Mater.* **1995**, *4*, 1073.
(12) Zhou, D.; Gruen, D. M.; Qin, L. C.; McCauley, T. G.; Krauss, A. R. *J. Appl. Phys.* **1998**, *84*, 1981.
(13) Gruen, D. M. *Annu. Rev. Mater. Sci.* **1999**, *29*, 211.
(14) Rao, A. M.; Richter, E.; Bandow, S.; Chase, B.; Eklund, P. C.; Williams, K. A.; Fang, S.; Subbaswamy, K. R.; Menon, M.; Thess, A.; Smalley, R. E.; Dresselhaus, G.; Dressehaus, M. S. *Science (Washington, D.C.)* **1997**, *75*, 187.
(15) Ferrari, A. C.; Robertson, J. *Phys. Rev. B* **2000**, *61*, 14095.
(16) Ferrari, A. C.; Robertson, J. *Phys. Rev. B* **2001**, *63*, 121405(R).
(17) Pfeiffer, R.; Kuzmany, H.; Salk, N.; Gunther, B. *Appl. Phys. Lett.* **2003**, *82*, 4149.
(18) Ferrari, A. C.; Robertson, J. *Phys. Rev. B* **2001**, *64*, 075414.
(19) Yarbrough, W. A.; Messier, R. *Science (Washington, D.C.)* **1990**, *247*, 688.
(20) Shroder R. E.; Nemanich R. J.; Glass, J. T. *Phys. Rev. B* **1990**, *41*, 3738.
(21) Parr, R. G.; Yang, W. *Density Functional Theory of Atoms and Molecules*; Oxford University Press: New York, 1989.
(22) Labanowski, J. K.; Anzelm, W. J. *Density Functional Methods in Chemistry*; Springer-Verlag: New York, 1991.
(23) Becke, A. D. *J. Chem. Phys.* **1993**, *98*, 5648.
(24) Fuente, E.; Menendez J. A.; Diez M. A.; Suarez D.; Montes-Moran M. A. *J. Phys. Chem.* **2003**, *107*, 6350.
(25) Neugebauer, J.; Reiher, M. B.; Hess, A. *J. Chem. Phys.* **2002**, *117*, 8623.
(26) Martin, J.; Montero, S. *J. Chem. Phys.* **1984**, *80*, 4610.
(27) Orduna, M. F.; del Olmo, A.; Domingo, C.; Montero, S. *J. Mol. Struct.* **1986**, *142*, 201.
(28) Schrotter, H. W.; Klockner, H. W. In *Raman Spectroscopy of Gases and Liquids*; Weber, A., Ed.; Springer: Berlin, 1979; pp 123−166.
(29) Placzek, G. *Z. Phys.* **1931**, *70*, 84.
(30) Furukawa, Y.; Takeucki H.; Harada I.; Tasumi, M. *Bull. Chem. Soc. Jpn.* **1983**, *56*, 392.
(31) Squillacote, M. E.; Sheridan, R. S.; Chapman, O. L.; Anet, F. A. L. *J. Am. Chem. Soc.* **1979**, *101*, 3657.
(32) Xie, R. H.; Bryant, G. W.; Smith, V. H., Jr. *Rhys. Rev. B* **2003**, *67*, 155404.
(33) Long, D. A. *Raman Spectroscopy*; McGraw-Hill: New York, 1977.
(34) Frisch, M. J.; Trucks, G. W.; Schlegel, H. B.; Scuseria, G. E.; Robb, M. A.; Cheeseman, J. R.; Zakrzewski, V. G.; Montgomery, J. A., Jr.; Stratmann, R. E.; Burant, J. C.; Dapprich, S.; Millam, J. M.; Daniels, A. D.; Kudin, K. N.; Strain, M. C.; Farkas, O.; Tomasi, J.; Barone, V.; Cossi, M.; Cammi, R.; Mennucci, B.; Pomelli, C.; Adamo, C.; Clifford, S.; Ochterski, J.; Petersson, G. A.; Ayala, P. Y.; Cui, Q.; Morokuma, K.; Malick, D. K.; Rabuck, A. D.; Raghavachari, K.; Foresman, J. B.; Cioslowski, J.; Ortiz, J. V.; Baboul, A. G.; Stefanov, B. B.; Liu, G.; Liashenko, A.; Piskorz, P.; Komaromi, I.; Gomperts, R.; Martin, R. L.; Fox, D. J.; Keith, T.; Al-Laham, M. A.; Peng, C. Y.; Nanayakkara, A.; Challacombe, M.; Gill, P. M. W.; Johnson, B.; Chen, W.; Wong, M. W.; Andres, J. L.; Gonzalez, C.; Head-Gordon, M.; Replogle, E. S.; Pople, J. A. *Gaussian 98*, Revision A.9; Gaussian, Inc.: Pittsburgh, PA, 1998.
(35) McDowell, S. A. C.; Amos, R. D.; Handy, N. C. *Chem. Phys. Lett.* **1995**, *235*, 1.
(36) Harada, I.; Furukawa Y.; Tasumi, M.; Shirakawa, H.; Ikeda, S. *J. Chem. Phys.* **1980**, *73*, 4746.
(37) Schuger, F. B.; Kuzmany, H. *J. Chem. Phys.* **1981**, *74*, 953.
(38) Kuzmany, H.; Pfeiffer, R.; Salk, N.; Gunther, B. *Carbon* **2004**, *42*, 911.
(39) Matus, M.; Kuzmany, H. *Appl. Phys. A* **1993**, *56*, 241.

(40) Liu, Y. L.; Jiang, Y. J.; Liu, J. Q.; Mo, Y. J.; Xie, S. S.; Zhang, Z. B.; Quan, S. F. *Phys. Rev. B* **1994**, *49*, 5058.
(41) Haufler, R. E.; Conceicao, J.; Chibante, L. P. F.; Chai, Y.; Byrne, N. E.; Flanagan, S.; Haley, M. M.; et al. *J. Phys. Chem.* **1990**, *94*, 8634.
(42) Howard, J. B.; McKinnon, J. T.; Makarovsky, Y.; Lafleur, A. L.; Johnson, M. E. *Nature* **1991**, *352*, 139.
(43) Lee, S. T.; Lin, Z. D.; Jiang, X. *Mater. Sci. Eng.* **1999**, *25*, 123.
(44) Orwa, J. O.; Prawer, S.; Jamieson, D. N.; Peng, J. L.; McCallum, J. C.; Nugent, K. W.; Li, Y. J.; Bursill, L. A. *J. Appl. Phys.* **2001**, *90*, 3007.
(45) Zhou, X. T.; Meng, X. M.; Meng, F. Y.; Li, Q.; Bello, I.; Lee, C. S.; Lee, S. T. *Diamond. Relat. Mater.* **2003**, *12*, 1640.
(46) Lin-Chung, P. J. *Phys. Rev. B* **1994**, *50*, 16905.
(47) Wang, C. Z.; Ho, K. M. *Phys. Rev. Lett.* **1993**, *71*, 1184.